Journal of Biomedical Optics

BiomedicalOptics.SPIEDigitalLibrary.org

Delineating the anatomy of the ciliary body using hybrid optical and photoacoustic imaging

George J. Tserevelakis
Stella Avtzi
Miltiadis K. Tsilimbaris
Giannis Zacharakis

SPIE.

George J. Tserevelakis, Stella Avtzi, Miltiadis K. Tsilimbaris, Giannis Zacharakis, "Delineating the anatomy of the ciliary body using hybrid optical and photoacoustic imaging," *J. Biomed. Opt.* **22**(6), 060501 (2017), doi: 10.1117/1.JBO.22.6.060501.

Delineating the anatomy of the ciliary body using hybrid optical and photoacoustic imaging

George J. Tserevelakis,[a,†] Stella Avtzi,[a,†] Miltiadis K. Tsilimbaris,[b] and Giannis Zacharakis[a,*]
[a]Foundation for Research and Technology Hellas, Institute of Electronic Structure and Laser, Heraklion, Crete, Greece
[b]University of Crete, School of Medicine, Laboratory of Vision and Optics, Heraklion, Crete, Greece

Abstract. We demonstrate the application of an extended field of view hybrid microscope, integrating distinct optical and photoacoustic (PA) contrast modes, for the precise three-dimensional anatomy delineation of the ciliary body/iris structures in healthy rabbit eyes *ex vivo*. The glutaraldehyde-induced autofluorescence and the intrinsic PA signals provided by each of the employed imaging modalities were characterized by a high spatial complementarity, offering thus rich morphological information regarding the pars plana and pars plicata ciliary body portions, the iris, as well as, the attached zonule fiber strands. The bimodal microscopy approach presented could find application on studies involving the ocular accommodation mechanism or pathological ciliary body conditions, as a powerful diagnostic technique contributing to the understanding of ocular physiology and function. [DOI: 10.1117/1.JBO.22.6.060501]

Keywords: ciliary body; eye; photoacoustic; imaging; microscopy; multimodal.

Paper 170101LRR received Feb. 12, 2017; accepted for publication May 23, 2017; published online Jun. 14, 2017.

The ciliary body is an ocular structure being responsible for two important functions: the secretion of aqueous humor in the anterior chamber by the epithelium cells and the accommodation of the eye through the control of the lens shape.[1] Due to its high significance in ophthalmology and vision science, several studies have attempted in the past to describe its anatomy and physiological function using mainly scanning electron microscopy (SEM),[2,3] which has been considered advantageous over traditional light imaging methods for such a case. Recently, however, the imaging community's interest has been directed to the development and application of hybrid microscopy instruments incorporating photoacoustic (PA) contrast modalities together with well-established optical techniques, to collect complementary information regarding the sample under observation.[4–6] As far as ocular imaging is concerned, a limited number of such high-resolution multimodal systems have been employed for the *in vivo* imaging of the retinal region, by combining the PA modality with state-of-the-art medical diagnostic tools, such as optical coherence tomography[7,8] and fluorescein angiography.[9] Furthermore, PA contrast has been effectively combined with ultrasound imaging to reveal anatomical information of several ocular components, such as ciliary body and choroid in pig eyes *ex vivo*.[10] In addition, another *ex vivo* study has imaged successfully retinal and ciliary body specimens, by exploiting both of the simultaneously generated PA and autofluorescence (AF) signals, following the excitation by a single-laser source.[11] Nevertheless, this approach was limited to an extremely small field of view, in the order of (1.5×1.5) mm^2, not allowing for the extraction of useful three-dimensional (3-D) anatomical information as to the whole ciliary body/iris/zonular fibrils system. Moreover, despite its admittedly high complementarity degree, the acquired AF contrast was highly questionable regarding its exact origin, and in any case, was restricted exclusively to the surface of the pigmented epithelium of the excised specimen.

Herewith, we present the application of an extended field of view hybrid microscope, integrating distinct optical and PA contrast modes, for the precise anatomical delineation of the ciliary body and iris structures. To demonstrate the capabilities of this imaging system, we used tissue specimens enucleated from healthy rabbit eyes (European rabbit—*Oryctolagus cuniculus*). Following the enucleation, two small holes were opened in each side of the eye bulb to facilitate the distribution of the fixation medium into the eye. The samples were submerged in 2.5% glutaraldehyde solution, serving as an AF inducing agent, as well as, sterilization and preservation medium and stayed overnight. Prior to the measurements, the eye bulb was sectioned in two parts, and the anterior segment was immobilized on a standard 170-μm-thick coverslip glass (with the rear side of the specimen facing its surface) using 2% concentration agar solution to avoid any drifting effects during the imaging procedure.

Figure 1(a) shows a schematic representation of the anterior segment of the eye from a posterior perspective (as looking from the retina) displaying several anatomical features of the ciliary body and the crystalline lens. Figure 1(b) shows a bright-field view of a bisected anterior segment specimen with the crystalline lens removed prior to the imaging session. The inner surface of the eye appears to be completely dark due to the highly absorptive retinal pigmented epithelium layer, hindering a detailed anatomical inspection through direct optical observation. The custom-developed hybrid microscopy setup shown in Fig. 1(c) integrates two distinct excitation paths, each of them dedicated for the AF and PA imaging mode, respectively. The AF imaging path employs a compact CW diode-pumped laser module (CPS450, Thorlabs, Newton, New Jersey; output power 4.5 mW) emitting at 450 nm, as an excitation source. Due to its highly elliptical shape, the beam is spatially filtered using an optical system consisting of two positive lenses (L1 and L2) and a 50-μm-diameter pinhole to improve its quality. The filtered radiation is further attenuated after passing through a set of neutral density filters, to avoid any photodamage effects on the examined specimen. The beam is subsequently reflected by a long-pass dichroic mirror (DMLP505, Thorlabs, Newton, New Jersey; cutoff wavelength: 505 nm) and guided into a properly modified inverted optical microscope (Labovert, Leitz, Wetzlar, Germany), following a 6× expansion by a telescope

*Address all correspondence to: Giannis Zacharakis, E-mail: zahari@iesl.forth.gr

†These authors contributed equally to this work.

1083-3668/2017/$25.00 © 2017 SPIE

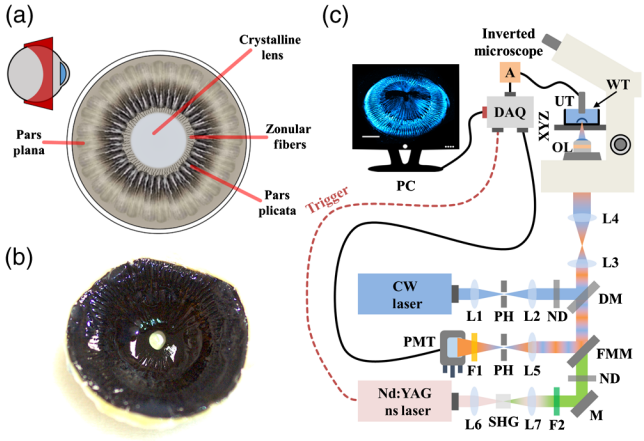

Fig. 1 Specimen's anatomy and hybrid imaging apparatus. (a) Schematic representation of the anterior eye segment from a posterior perspective. (b) Bright-field view of a healthy rabbit eye that has been bisected in the coronal plane (crystalline lens removed). (c) Hybrid microscopy setup integrating optical and PA modes. Abbreviations: L(1-7), lenses; PH, pinhole; ND, neutral density filters; DM, dichroic mirror; FMM, flip mount mirror; F1, long-pass filter; PMT, photomultiplier tube; SHG, second harmonic generation crystal; F2, bandpass filter; M, mirror; OL, objective lens; XYZ, 3-D translation stages; WT, water tank; UT, ultrasonic transducer; A, amplifier; DAQ, data acquisition card; and PC, recording computer.

(L3 and L4). An objective lens (Achromat 8×, LOMO, St. Petersburg, Russia; air immersion; NA: 0.2) focuses the light directly on the rear side of the anterior segment specimen, which is placed at the bottom of an optically transparent water tank. The tank is attached on a high precision 3-D translational motion system consisting of a fast motorized XY scanning stage (8MTF-75LS05, Standa, Vilinius, Lithuania) and the built-in manual Z-control of the microscope, through which the imaging focal plane is selected. A part of the back-scattered fluorescence radiation is collected by the objective, transmitted through the dichroic mirror, and focused (lens L5) on a 25-μm-diameter pinhole, to reject the out-of-focus incoming light. A long-pass filter (LP03-532RU-25, Semrock Inc., Rochester, New York; edge wavelength: 532 nm) is placed behind the pinhole to cut off the reflected excitation radiation and isolate exclusively the in-focus emitted AF, which is finally detected by a photomultiplier tube (H6780-20, Hamamatsu, Hamamatsu City, Japan). The generated signals are recorded by a high-speed data acquisition (DAQ) card (PCIe-9852, ADLINK, Taipei, Taiwan; sampling rate: 200 MS/s; bandwidth: 90 MHz) and subsequently stored in a computer, following the averaging of 40 measurements for SNR improvement. A typical 400×400 pixels optical imaging session requires around 15 min to complete by the XY stages, which raster scan the specimen over the beam focus.

Regarding the PA imaging path, a variable repetition rate pulsed Nd:YAG laser emitting at 1064 nm (QIR-1064-200-S, CrystaLaser LC, Reno, Nevada; pulse energy: 29.4 μJ, pulse duration: 10 ns, selected repetition rate: 6.78 kHz) is employed as an excitation source. The beam is focused on a Lithium triborate (LBO) second harmonic generation (SHG) crystal (Castech Inc., Fuzhou, China) to be partially transformed into a 532-nm wavelength and subsequently collimated by a second lens (L6 and L7, respectively). A bandpass filter (FF01-531/40-25, Semrock, Rochester, New York) is used to reject the remaining fundamental infrared radiation, whereas the transmitted visible wavelength is adequately attenuated through a second set of neutral density filters. With the AF reflecting mirror flipped out of the optical path, the PA excitation beam passes through the dichroic mirror and the telescope of the system, to be focused by the same objective lens on the specimen under observation. The induced PA waves are detected by a 20-MHz central frequency spherically focused ultrasonic transducer (V373-SU, Olympus, Tokyo, Japan; effective bandwidth: 13 to 33 MHz, focal distance: 32 mm), which is immersed into the tank in a confocal and coaxial configuration with respect to the optical focus. The distilled water in the tank serves as a coupling medium between the source and the detector, ensuring the effective PA waves propagation. The generated signals are enhanced by a low noise RF amplifier (AU-1291, Miteq, New York; gain: 63 dB) and recorded by the DAQ card of the system, which is synchronized with the laser trigger signal. The raster scanning of the specimen is similarly achieved using the motorized XY stages of the microscope and requires around 20 min to complete (400×400 pixels, 16 averaged waveforms). To generate a 3-D PA imaging reconstruction, the recorded time-domain signal for each lateral scanning position was Hilbert-transformed, and its modulus was assigned directly to the respective voxel intensity. The data processing, as well as, the coregistration of the recorded images was performed with MATLAB™ and ImageJ Java-based software.

Figure 2(a) shows a PA imaging reconstruction of a whole ciliary body/iris specimen excised from a rabbit eye, in posterior perspective view. In this case, the recorded volume was $(16 \times 16 \times 3)$ mm^3, whereas the respective voxel size was equal to $(40 \times 40 \times 15)$ μm^3. Such an extended field of view image provides high-resolution anatomical information through the PA signals generation, as a result of the strong absorption of the incident visible radiation by the pigmented epithelium layer covering the whole specimen. More specifically, the outer region (1) in red color corresponds to the pars plana (flat portion) of the ciliary body, having a typical smooth surface morphology. The inner region (2) in green represents the pars plicata (folded portion), located anterior to the pars plana and posterior to the iris of the eye. As it is clear from the PA reconstruction, the pars plicata is characterized by several radially oriented ridges pointing toward the pupil, named ciliary processes, which are known to secrete aqueous humor into the anterior eye chamber. Furthermore, it is apparent that the PA signal amplitude presents a consistent periodic modulation along the circumference of the pars plicata, revealing thus the tips of the processes as high signal regions, and the valleys lying between them as locations of low or negligible signal. Finally, the area (3) marked with yellow color represents the iris of the eye, which appears as a round region of ~10 mm in diameter. It is noteworthy that the iris generates lower signals compared to the surrounding ciliary body; however, this effect can be attributed to the decreased local energy fluence in this region, as a result of the excitation beam's divergence, rather than the significantly different absorption properties of the tissue. A side view of the PA reconstruction for a central ~1-mm-width slice (indicated with a dashed box) is presented in Fig. 2(b), to provide an additional anatomical aspect of the specimen under investigation. This image reveals clearly the ciliary body's axial position in respect to the iris, appearing to protrude by a vertical distance in the order of 2 mm. The zero signal area located in the center of the iris region corresponds to the

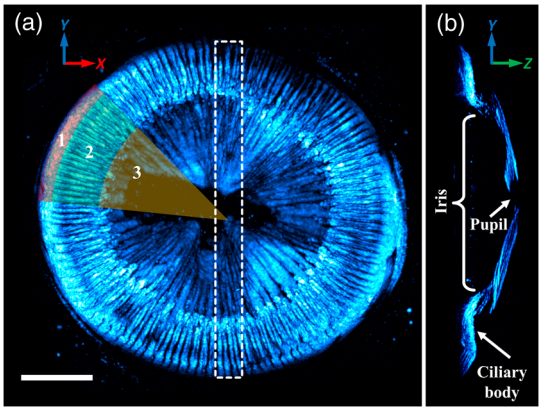

Fig. 2 PA reconstruction of a whole ciliary body/iris tissue specimen enucleated from a rabbit eye. (a) Posterior perspective view of the anterior segment reveals the (1) pars plana, (2) pars plicata, and (3) iris parts. (b) Side view of the region indicated with the dashed box in (a) provides additional anatomical information of the specimen. Scale bar is equal to 3 mm.

pupil, which allows the incoming light to pass into the eye. Having delineated the coarse anatomy of a whole ciliary body/iris specimen using exclusively the PA contrast mode, we proceeded to the hybrid PA and optical imaging of an anterior segment slice which was bisected from an additional eye bulb. Figure 3(a) shows a maximum amplitude projection PA image of the scanned area, having lateral dimensions (3.86×5.93) mm^2, with a respective pixel size of (20×20) μm^2. The top part of the image depicts the ciliary processes and the valleys between them, as well as, the surrounding smooth pars plana region in high spatial resolution and contrast. Moreover, the lower half of the image reveals clearly the iridial processes, which extend radially along the posterior surface of the iris, forming continuations of the ciliary processes. The sequential

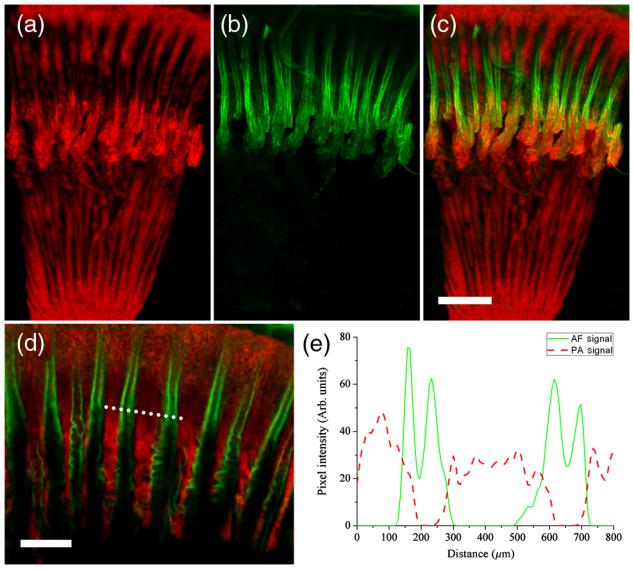

Fig. 3 Hybrid imaging of rabbit eye's anterior segment. (a) PA image of ciliary body and iris. (b) Glutaraldehyde-induced AF image revealing the zonular fibrils. (c) Merged bimodal reconstruction. Scale bar is equal to 1 mm. (d) High-resolution bimodal image of the ciliary processes and zonular fibrils in an additional specimen. (e) Plot of the signal intensity values along the dotted line shown in (d). Scale bar is equal to 0.5 mm.

AF imaging session of the same region is presented explicitly in Fig. 3(b), to reveal several fibrous structures following straight or multifolded paths as they extend along the ciliary body. It is noteworthy to mention that these signals appeared to be highly specific in space, since no remarkable AF contribution was observed by other regions of the specimen. Basic anatomical knowledge of the eye indicates that this characteristic arrangement of fibers corresponds to a segment of the ciliary zonule (or zonule of Zinn), a ring of fibrous strands that connects the ciliary body to the crystalline lens, playing an important role during accommodation. The main component of these fibrous strands is fibrillin,[12,13] a glycoprotein present virtually in all dynamic connective tissues.[14] On the other hand, the glutaraldehyde fixation medium that was used as preservative following the eye enucleation, is known to react with several biomolecules, such as proteins and peptides to generate high quantum yield fluorophores.[15] Therefore, a possible explanation of the fluorogenic mechanism regarding the investigated specimens could be the fibrillin cross-linking with glutaraldehyde resulting in the emission of strong AF signals. This hypothesis is further supported by the absolute absence of any fluorescence from samples that had not been embedded in glutaraldehyde prior the optical imaging session. Figure 3(c) is the merged bimodal reconstruction of the specimen through the employed PA (red) and optical (green) contrast modes. The coregistered image shows clearly the fiber strands entering the ciliary valleys closely attached to the lateral walls of the protruding ciliary processes, to end up within the depths of the pigmented epithelium covering the pars plana region. It is worth mentioning that such a detailed description of the ciliary body's anatomy is found in excellent agreement with the relevant SEM[1–3] studies, providing in this manner, additional evidence regarding the claimed imaging contrast sources. As a last step, we have imaged a ciliary body section using both modalities, this time by zooming in a region at the border between pars plana and pars plicata portions as explicitly shown in Fig. 3(d). For this image, the scanned area was (2.85×2.35) mm^2, whereas the respective pixel size was as small as (7.5×7.5) μm^2. To provide an approximate lateral size estimation of the imaged components, we have plotted the signal intensity values along the dotted line of the figure. The PA curve (red dashed line) of the graph presented in Fig. 3(e) corresponds to a full width at half maximum value in the order of 300 μm for the central ciliary process. On the other hand, the respective width of the AF peaks (green line) ranges between 35 and 55 μm, which constitutes a good measure of the zonular fiber strands diameter. Once more, both of the calculated values are very close to the relative bibliographical references as to the dimensions of these ocular structures in similar rabbit eye specimens using SEM,[16,17] validating thus the reliability of the proposed imaging methodology.

In conclusion, we have presented the application of a prototype hybrid optical and PA microscopy system for the detailed, structural imaging of the ciliary body/iris tissue in rabbit eye specimens. We have demonstrated that the signals provided by each of the integrated modalities are spatially complementary and have the potential to offer high contrast anatomical information regarding the pars plana and pars plicata ciliary body portions, the iris, as well as, the attached zonule fiber strands. Nevertheless, further histopathological studies have to be performed to verify the exact imaging contrast source for each case.

To boost the current microscope's performance, in terms of spatial and temporal resolution, SNR, and contrast specificity,

several technical improvements can be implemented in a future upgraded version of the imaging setup. First of all, the integration of a fast galvo mirror scanner could dramatically decrease the acquisition time down to several seconds, enabling thus high-resolution 3-D fluorescence imaging capabilities. In addition to this, a broad detection bandwidth ultrasonic transducer would significantly improve the axial resolving power of the PA modality to permit a more detailed investigation of the ocular features of interest. Furthermore, the current hybrid PA setup could be further combined with more imaging techniques, such as optical coherence tomography, harmonics generation imaging, or even coherent anti-Stokes Raman scattering microscopy, to obtain information regarding the specific molecular composition of different ocular regions. On top of this, an adaptive optics subsystem coupled with an epi-illumination PA imaging apparatus could enhance the imaging quality through highly scattering media of the eye, such as sclera, allowing for whole eye imaging without the necessity of a specimen's bisection. Finally, multispectral PA excitation using NIR, visible, and UV wavelengths would offer the imaging capability of several ocular components with distinct optical absorption properties, such as the cornea, the crystalline lens, the choroid layer, etc.

We anticipate that the bimodal imaging approach introduced in this work will be further exploited in studies involving the accommodation mechanism and pathological ciliary body conditions as a powerful diagnostic tool contributing to the comprehensive understanding of ocular physiology and function.

Disclosures

The authors declare no competing financial interests.

Acknowledgments

The authors acknowledge the financial support through the GSRT project Skin-DOCTor (No. 1778) implemented under the Action ARISTEIA, in the framework of Operational Program Education and Lifelong Learning cofunded by the European Social Fund and National Resources. Also, financial support was provided by the EU FP7 Marie Curie ITN OILTEBIA project, PITN-GA-2012-317526 and H2020 Laserlab Europe (EC-GA 654148) project. This work was completed during the master program Optics and Vision of School of Medicine—University of Crete. The authors wish to thank Ms. Styliani V. Blazaki and Dr. Irini Naoumidi for providing rabbit eye specimens.

References

1. E. R. Tamm and E. Lütjen-Drecoll, "Ciliary body," *Microsc. Res. Tech.* **33**(5), 390–439 (1996).
2. N. Bornfeld et al., "Scanning electron microscopy of the zonule of Zinn—I. Human eyes," *Graefes Arch. Clin. Exp. Ophthalmol.* **192**(2), 117–129 (1974).
3. J. W. Rohen, "Scanning electron microscopic studies of the zonular apparatus in human and monkey eyes," *Invest. Ophthalmol. Visual Sci.* **18**(2), 133–144 (1979).
4. B. Rao et al., "Integrated photoacoustic, confocal, and two-photon microscope," *J. Biomed. Opt.* **19**(3), 036002 (2014).
5. G. J. Tserevelakis, M. Tsagkaraki, and G. Zacharakis, "Hybrid photoacoustic and optical imaging of pigments in vegetative tissues," *J. Microsc.* **263**(3), 300–306 (2016).
6. D. Soliman et al., "Combining microscopy with mesoscopy using optical and optoacoustic label-free modes," *Sci. Rep.* **5**, 12902 (2015).
7. S. Jiao et al., "Photoacoustic ophthalmoscopy for *in vivo* retinal imaging," *Opt. Express* **18**(4), 3967–3972 (2010).
8. Q. Wei et al., "Image chorioretinal vasculature in albino rats using photoacoustic ophthalmoscopy," *J. Mod. Opt.* **58**(21), 1997–2001 (2011).
9. W. Song et al., "Integrating photoacoustic ophthalmoscopy with scanning laser ophthalmoscopy, optical coherence tomography, and fluorescein angiography for a multimodal retinal imaging platform," *J. Biomed. Opt.* **17**(6), 061206 (2012).
10. R. H. Silverman et al., "High-resolution photoacoustic imaging of ocular tissues," *Ultrasound Med. Biol.* **36**(5), 733–742 (2010).
11. X. Zhang et al., "Simultaneous dual molecular contrasts provided by the absorbed photons in photoacoustic microscopy," *Opt. Lett.* **35**(23), 4018–4020 (2010).
12. F. Skovby and J. P. Kraus, "Homocystinuria," in *Connective Tissue and Its Heritable Disorders: Molecular, Genetic, and Medical Aspects*, P. M. Royce and B. Steinmann, Eds., 2nd ed., pp. 636, Wiley-Liss, New York (2002).
13. E. R. Berman, *Biochemistry of the Eye (Perspectives in Vision Research)*, 1st ed., pp. 299–300, Plenum Press, New York (1991).
14. C. M. Kielty et al., "Fibrillin: from microfibril assembly to biomechanical function," *Philos. Trans. R. Soc. B* **357**(1418), 207–217 (2002).
15. K. Lee et al., "Autofluorescence generation and elimination: a lesson from glutaraldehyde," *Chem. Commun.* **49**(29), 3028–3030 (2013).
16. M. Davanger and O. Ö. Pedersen, "The ciliary body and the suspension of the lens in rabbits: a scanning electron microscopy study," *Acta Ophthalmol.* **56**(1), 127–138 (1978).
17. J. C. Morrison, M. P. DeFrank, and E. M. Van Buskirk, "Regional microvascular anatomy of the rabbit ciliary body," *Invest. Ophthalmol. Visual Sci.* **28**(8), 1314–1324 (1987).